PHILOSOPHICAL TRANSACTIONS OF THE ROYAL SOCIETY B BIOLOGICAL SCIENCES

Excitation, Oscillations and Wave Propagation in a G-Protein-Based Model of Signal Transduction in Dictyostelium discoideum

Yuanhua Tang and Hans G. Othmer

Phil. Trans. R. Soc. Lond. B 1995 **349**, 179-195
doi: 10.1098/rstb.1995.0102

Excitation, oscillations and wave propagation in a G-protein-based model of signal transduction in *Dictyostelium discoideum*

YUANHUA TANG* AND HANS G. OTHMER

Department of Mathematics, University of Utah, Salt Lake City, Utah 84112, U.S.A.

SUMMARY

In an earlier paper (Tang & Othmer 1994 *Math. Biosci* **120**, 25–76), we developed a G-protein-based model for signal transduction in the cellular slime mould *Dictyostelium discoideum* and showed that it can account for the results from perfusion experiments done by Devreotes and coworkers (Devreotes *et al.* 1979 *J. Cell.* **80**, 300–309; Devreotes & Steck 1979 *J. Cell Biol.* **80**, 300–309; Dinauer *et al.* 1980 *J. Cell Biol.* **86**, 537–561). The primary experimental observables are the amounts of cAMP secreted and the time scale of adaptation in response to various stimuli, and we showed that the predictions of the model agree well with the observations. Adaptation in the model arises from dual receptor-mediated pathways, one of which produces a stimulatory G protein G_s and the other of which produces an inhibitory G protein G_i.

In this paper we use the model to simulate the suspension experiments of Gerisch & Wick (1975 *Biochem. biophys. Res. Commun.* **65**, 364–370) and the experiments done in cell cultures on Petri dishes (Tomchik & Devreotes 1981 *Science, Wash.* **212**, 443–446). The model predicts excitation to cAMP stimuli, sustained oscillations, or spiral waves and target patterns, depending on the developmental stage of the cells and experimental conditions. The interaction between different pacemakers is also studied.

1. INTRODUCTION

The cellular slime mould *Dictyostelium discoideum* (Dd) is a model system that is used for the study of many developmental processes, including signal transduction, gene transcription control, cell–cell interactions and spatial pattern formation (Devreotes 1989; Loomis 1992; Schaap & Wang 1993). In a previous paper (Tang & Othmer 1994*a*) (hereafter referred to as I), we proposed a model for signal transduction based on G proteins that adequately reproduces experimental results obtained from perfusion experiments. In particular, the model reproduces the observed adaptation to constant cAMP stimuli while retaining sensitivity to further stimuli, it exhibits the observed amplification of extracellular cAMP stimuli and it correctly reproduces the time scale of the response to constant stimuli and the subsequent adaptation to such stimuli. Thus the model provides an adequate representation of the input–output behaviour of an individual cell, and one can use it to investigate various aspects of the collective behaviour of cell populations under different experimental conditions. In this paper we extend the single cell model to describe the dynamics of two such situations: (i) cell suspensions, in which there is no spatial variation of extracellular cAMP, and (ii) spatially distributed systems, in which cell-to-cell signalling is accomplished via travelling waves of cAMP. Other aspects, such as the details of signal detection and orientation in aggregation fields (Dallon & Othmer 1995*a*) and pattern formation in the slug stage (Othmer *et al.* 1995) are currently under investigation. Previous work on the aspects treated here, with other models for transduction and adaptation, are reviewed in Monk & Othmer (1990).

One approach to understanding the collective behaviour of a population of cells is via the suspension experiment, in which cells are suspended in a well mixed solution (Gerisch & Wick 1975). Two types of behaviour are observed in such experiments when using cells that are 4–8 h post-starvation: (i) an excitable response to a cAMP stimulus and (ii) temporal oscillations of both extracellular and intracellular cAMP (Durston 1973; Gerisch & Hess 1974). In case (i) the cells are relay-competent and in case (ii) they are oscillatory. The relay-competent cells can amplify the stimulus signal by a factor of from ten to several hundred. The refractory period varies from greater than 7 min in early aggregation cells to less than 3 min in late stage cells. The typical period of the oscillation is about 5–10 min. The peak extracellular

* Current address: Department of Physiology and Biophysics, Cornell University Medical College, New York, New York 10021, U.S.A.

cAMP concentrations are in the range of 1–5 μM during oscillation, whereas the intracellular cAMP concentration varies from 10 to 30 μM (Gerisch & Wick 1975; Gerisch *et al.* 1979).

If relay-competent Dd cells are spread over an agar surface, two-dimensional waves of extracellular and intracellular cAMP can be observed (Tomchik & Devreotes 1981; Newell 1983; Foerster *et al.* 1990). The waves of extracellular cAMP travel across the field in the form of either target patterns (expanding concentric waves) or spiral waves with rotating cores. Different types of interacting wave patterns, such as interacting target patterns and coexisting spiral waves of the same or of the opposite rotation, are found experimentally.

The extracellular cAMP wave rises from a level of less than about 0.01 μM to a peak value of around 1 μM in a medium with a cell density of 10^6 cells per square centimetre. In either a spiral wave or a concentric wave, the distance between two travelling fronts is 1–4 mm. The speed of these waves is approximately 300–600 μM min^{-1} and the time between two successive wave fronts is 6–10 min (Tomchik & Devreotes 1981; Siegert & Weijer 1989). The travelling cAMP waves serve as the chemotactic signal to induce aggregation of the cells, which move towards the centre at about 20 μm min^{-1}. Morphogenesis is organized primarily by cAMP waves at this stage (Robertson *et al.* 1972; Clark & Steck 1979).

In a mathematical model the variation of a parameter related to biochemical properties of a cell can be used to simulate changes in the developmental stage of that cell. One such parameter is the amount of adenylate cyclase present. It is known that as cells progress through the developmental stages they increase the expression of the gene coding for adenylate cyclase (Schaap & Wang 1993). In our model, as the amount of adenylate cyclase increases the cells first show little capacity for signal amplification, then they become excitable (and relay-competent) in response to cAMP stimuli. When the parameter exceeds a critical value, an oscillatory response ensues. If cells in the excitable stage are distributed on agar, the resulting medium is excitable and can support various types of travelling waves. Oscillatory cells can serve as pacemakers (DeYoung *et al.* 1988) to organize concentric waves, or spiral waves may exist without pacemakers. Numerical simulations from our model agree well with the experimental results in each of the foregoing aspects.

An outline of this paper is as follows. In section 2 we describe the signal transduction model developed in Tang & Othmer (1994*a*), we show how it can be reduced further and we develop the governing equations for suspensions. A bifurcation analysis and numerical simulations for the local dynamics are given in section 3. In section 4 spatial variations of cAMP concentration are introduced, which lead to a partial differential equation coupled to several ordinary differential equations. This system is used to study one-dimensional and two-dimensional waves. New experimental results that bear on the validity of our model and others are discussed in the final section.

2. THE MODEL EQUATIONS FOR SPATIALLY UNIFORM SYSTEMS

(*a*) *A description of the model for signal transduction*

The network for the main steps in the transduction scheme used in the model developed in I is shown in figure 1. In the model there are three major pathways in the transduction of and adaptation to an extracellular perfusing cAMP signal (H) in perfusion experiments. In the stimulus pathway, cAMP binds to receptors R_s, and the complex HR_s catalyses the activation of the stimulatory G protein G'_s. This in turn binds with the inactive form of adenylate cyclase (UC) and produces the activated form of adenylate cyclase ($G'_s AC$). A GTPase activity intrinsic to the α subunit of the G protein terminates the activation. In the inhibitory pathway, an inhibitory G protein G'_i is produced by analogous steps. However, the symmetry between the pathways is broken at this point, because G'_i binds with HR_s, and in this bound form HR_5 cannot activate G_s. Finally in the pathway for the production and secretion of cAMP, the activated adenylate cyclase ($G'_s AC$) catalyses the turnover of ATP to intracellular cAMP ($cAMP_i$). $cAMP_i$ in turn is hydrolysed by intracellular phosphodiesterase (iPDE) or is secreted into the extracellular medium ($cAMP^*_o$). Here the asterisk on $cAMP^*_o$ is to distinguish the secreted cAMP from the stimulatory cAMP in the perfusion solution, which is denoted by H. The detailed

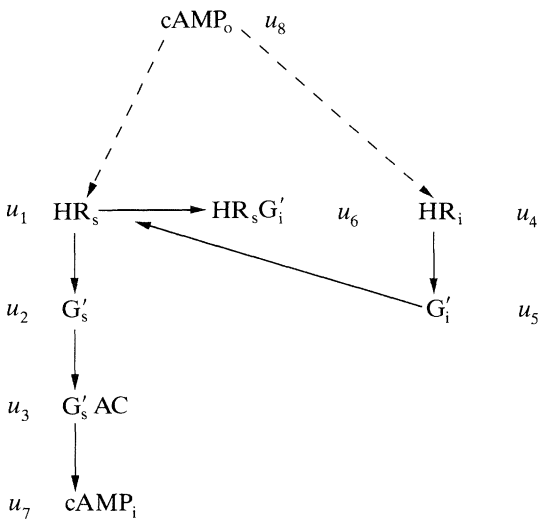

Figure 1. A schematic diagram of the interactions in the model. An extracellular cAMP stimulus serves both as the stimulus and as the inhibitory signal. Adaptation arises from the action of G'_i on the hormone receptor complex. Symbols: $cAMP_o$, extracellular cAMP; R_s, receptor for the stimulatory pathway; HR_s, hormone ($cAMP_o$)–receptor complex; G'_s, activated stimulatory G protein, $G'_s AC$, activated form of adenylate cyclase, $cAMP_i$, intracellular cAMP; R_i, cAMP receptor in the inhibitory pathway; HR_i, hormone–receptor complex in the inhibitory pathway; G'_i, activated form of the inhibitory G protein; $HR_sG'_s$, complex between HR_s and G'_s. The symbol u_j beside each species is the dimensionless concentration of that species. For details on the non-dimensionalization see I.

PHILOSOPHICAL TRANSACTIONS OF THE ROYAL SOCIETY B BIOLOGICAL SCIENCES

biochemical reactions as well as kinetic parameters involved are given in the following equations. Further details about this model can be found in our original paper (I) (Tang & Othmer 1994*a*).

(i) *The stimulus pathway*

$$\left.\begin{aligned}
&\mathrm{H}+\mathrm{R_s}\underset{k_{-1}}{\overset{k_1}{\rightleftharpoons}}\mathrm{HR_s}\\
&\mathrm{HR_s}+\mathrm{G_s}\underset{k_{-2}}{\overset{k_2}{\rightleftharpoons}}\mathrm{HR_sG_s}\\
&\mathrm{HR_sG_s}+\mathrm{GTP}\overset{\hat{k}_3}{\rightarrow}\mathrm{HR_s}+\mathrm{G_s'}+\mathrm{GDP}+\beta\gamma\\
&\mathrm{G_s'}+\mathrm{UC}\underset{k_{-4}}{\overset{k_4}{\rightleftharpoons}}\mathrm{G_s'AC}\\
&\mathrm{G_s'}\overset{k_5}{\rightarrow}\alpha_s\,\mathrm{GDP}+\mathrm{P_i}\\
&\mathrm{G_s'AC}\overset{k_5}{\rightarrow}\alpha_s\,\mathrm{GDP}+\mathrm{UC}+\mathrm{P_i}\\
&\alpha_s\,\mathrm{GDP}+\beta\gamma\overset{k_6}{\rightarrow}\mathrm{G_s}.
\end{aligned}\right\}\qquad(1)$$

(ii) *The inhibitory pathway*

$$\left.\begin{aligned}
&\mathrm{H}+\mathrm{R_i}\underset{h_{-1}}{\overset{h_1}{\rightleftharpoons}}\mathrm{HR_i}\\
&\mathrm{HR_i}+\mathrm{G_i}\underset{h_{-2}}{\overset{h_2}{\rightleftharpoons}}\mathrm{HR_iG_i}\\
&\mathrm{HR_iG_i}+\mathrm{GTP}\overset{\hat{h}_3}{\rightarrow}\mathrm{HR_i}+\mathrm{G_i'}+\mathrm{GDP}+\beta\gamma\\
&\mathrm{G_i'}+\mathrm{HR_s}\underset{h_{-4}}{\overset{h_4}{\rightleftharpoons}}\mathrm{HR_sG_i'}\\
&\mathrm{G_i'}\overset{h_5}{\rightarrow}\alpha_i\,GDP+P_i\\
&\mathrm{HR_sG_i'}\overset{h_6}{\rightarrow}\mathrm{H}+\mathrm{R_s}+\mathrm{G_i'}\\
&\mathrm{HR_sG_i'}\overset{h_5}{\rightarrow}\mathrm{HR_s}+\alpha_i\,\mathrm{GDP}+\mathrm{P_i}\\
&\alpha_i\,\mathrm{GDP}+\beta\gamma\overset{h_7}{\rightarrow}\mathrm{G_i}.
\end{aligned}\right\}\qquad(2)$$

(iii) *The production and secretion of intracellular cAMP*

$$\left.\begin{aligned}
&\mathrm{G_s'AC}+\mathrm{ATP}\underset{l_{-1}}{\overset{\hat{l}_1}{\rightleftharpoons}}\mathrm{G_s'AC-ATP}\\
&\mathrm{G_s'AC-ATP}\overset{l_2}{\rightarrow}\mathrm{cAMP_i}+\mathrm{G_s'AC}\\
&\mathrm{cAMP_i}+\mathrm{iPDE}\underset{l_{-3}}{\overset{l_3}{\rightleftharpoons}}\mathrm{cAMP_i-iPDE}\\
&\mathrm{cAMP_i-iPDE}\overset{l_4}{\rightarrow}\mathrm{AMP}+\mathrm{iPDE}\\
&\mathrm{cAMP_i}\overset{l_5}{\rightarrow}\mathrm{cAMP_o^*}.
\end{aligned}\right\}\qquad(3)$$

As we showed in I, this model can describe the input–output behaviour in the perfusion experiments very well. However, to better describe certain aspects of the oscillation experiments and the wave propagation studied in this paper, we introduce two modifications. The first is to introduce a low basal activity for the unactivated adenylate cyclase.

This basal activity of UC is responsible for the basal cAMP concentration in the cytoplasm in the absence of an extracellular signal. The symbols used for the secretion rate in I, l_5 and $l_5\gamma_5$, will no longer be used with the old meaning. Instead, we use l_5 and γ_5 for the basal enzymic activity of UC. The additional reaction steps introduced by the basal activity are

$$\left.\begin{aligned}
&\mathrm{UC}+\mathrm{ATP}\underset{l_{-5}}{\overset{l_5}{\rightleftharpoons}}\mathrm{UC-ATP}\\
&\mathrm{UC-ATP}\overset{l_5^*}{\rightarrow}\mathrm{cAMP_i}+\mathrm{UC}.
\end{aligned}\right\}\qquad(4)$$

The second modification is related to the first. Since cells usually need a basal intracellular cAMP concentration for normal functions, the secretion rate should be small at low cAMP concentrations. Cells should begin to secrete cAMP rapidly only when the intracellular cAMP concentration exceeds a threshold value. To model this, a nonlinear secretion function is required, and we accomplish this by using a switch on the secretion rate. We introduce the secretion function

$$dsr(\mathrm{cAMP_i})=\begin{cases}dsr_1*\mathrm{cAMP_i} & \text{if } \mathrm{cAMP_i}<dsw\\ dsr_2*(\mathrm{cAMP_i}-dsw)+dsr_1*dsw & \text{if } \mathrm{cAMP_i}>dsw\end{cases}\qquad(5)$$

and the secretion step

$$\mathrm{cAMP_i}\overset{dsr}{\rightarrow}\mathrm{cAMP_o^*},\qquad(6)$$

where dsr_1 is the basal secretion rate, dsr_2 is the active secretion rate, and dsw is the threshold concentration. The corresponding dimensionless parameters will be denoted as sr_1, sr_2, sw and sr. The piecewise linear character of the function $dsr(\cdot)$ can introduce difficulties for certain numerical schemes that require more smoothness than C^0. To circumvent this, we introduce a smoothed version of $dsr(\cdot)$ that uses a smooth spline interpolation between the linear functions in the neighbourhood of sw. Since the true secretion rate function is not known, this does not affect the validity of the model.

We shall use the symbols as were used in I to denote the dimensional and dimensionless variables. The definitions of and the relation between dimensional and dimensionless variables are given in table 1. If we simply carry over the equations for $u_1,\ldots u_6$ and u_8 from I, and modify the equation for u_7 in accordance with

PHILOSOPHICAL TRANSACTIONS OF THE ROYAL SOCIETY B BIOLOGICAL SCIENCES

Table 1. *Definition of and relation between dimensional and dimensionless variables*

	species	dimensional form	dimensionless form
stimulus pathway	$[HR_2]$	y_1	$u_1 = \dfrac{y_1}{[R_s]_T}$
	$[HR_s G_s]$	y_2	$v_1 = \dfrac{(k_{-2}+k_3)}{k_2[R_s]_T[T_s]_T} y_2$
	$[G_s']$	y_3	$u_2 = \dfrac{y_3}{[G_s]_T}$
	$[G_s' AC]$	y_4	$u_3 = \dfrac{y_4}{[UC]_T}$
	$[\alpha_s GDP]$	y_5	$v_2 = \dfrac{k_6}{k_5} y_5$
inhibitory pathway	$[HR_i]$	y_6	$u_4 = \dfrac{y_6}{[R_i]_T}$
	$[HR_i G_i]$	y_7	$v_3 = \dfrac{(h_{-2}+h_3)}{h_2[R_i]_T[G_i]_T} y_7$
	$[G_i']$	y_8	$u_5 = \dfrac{y_8}{[G_i]_T}$
	$[HR_s G_i']$	y_9	$u_6 = \dfrac{y_9}{[R_s]_T}$
	$[\alpha_i GDP]$	y_{10}	$v_4 = \dfrac{h_7}{h_5} y_{10}$
cAMP generation and secretion	$[G_s' AC—ATP]$	y_{11}	$v_5 = \dfrac{l_{-1}+l_2}{l_1[UC]_T} y_{11}$
	$[cAMP_i]$	y_{12}	$u_7 = \dfrac{y_{12}}{[iPDE]_T}$
	$[iPDE—cAMP_i]$	y_{13}	$v_6 = \dfrac{(l_{-3}+l_4)\, y_{13}}{l_3[iPDE]_T^2}$
	$[cAMP_o^*]$	y_{14}^*	$u_8^* = \dfrac{y_{14}^*}{[iPDE]_T}$
	time scale	t	$\tau = k_5 t$

the above, we arrive at the following system:

$$
\left.
\begin{aligned}
du_1/d\tau &= \alpha_H(\tau) - (\alpha_H(\tau)+\alpha_1)\, u_1 \\
&\quad + (\beta_5 - \alpha_H(\tau))\, u_6 - \beta_4 u_1 u_5, \\
du_2/d\tau &= \alpha_2 \alpha_3 c_1 u_1 - (1+\alpha_4)\, u_2 \\
&\quad - \alpha_2 \alpha_3 c_1 u_1 (u_2+u_3) + \alpha_4 u_2 u_3, \\
du_3/d\tau &= \alpha_4 u_2 - u_3 - \alpha_4 u_2 u_3, \\
du_4/d\tau &= \beta_H(\tau) - (\beta_H(\tau)+\beta_1)\, u_4, \\
du_5/d\tau &= \beta_2 \beta_3 c_2 u_4 - \beta_5 u_5 + \beta_6 c_3 u_6 \\
&\quad - c_3 \beta_4 u_1 u_5 - \beta_2 \beta_3 c_2 u_4 (u_5 + c_3 u_6), \\
du_6/d\tau &= -(\beta_5+\beta_6)\, u_6 + \beta_4 u_1 u_5, \\
du_7/d\tau &= \gamma_1 \gamma_2 u_3 - sr(u_7) - \gamma_4 u_7/(u_7+\gamma_3) \\
&\quad + \gamma_5 (1 - \Gamma_7 u_3), \\
du_8^*/d\tau &= sr(u_7).
\end{aligned}
\right\} \qquad (7)
$$

The reader may simply take these as the governing equations for the quantities shown in figure 1. The new dimensionless parameters introduced are $\gamma_5 = l_5[UC]_T A_c/(k_5[iPDE]_T V_c)$, $L_5 = (l_5 + l_5^*)/(l_5[ATP])$ and $\Gamma_7 = 1 + L_5$; $[\cdot]_T$ stands for the total enzyme concentration of that species within a cell. The dimensionless secretion rate is $sr_i = dsr_i/k_5$, $i = 1,2$. Estimates for these quantities are given later in this section. The other parameters, which were estimated in I, are given in table 2. In addition, we use $[\cdot]_T$ to represent the total concentration of a species and $H(t)$ to denote the cAMP stimulus.

There are five instances in table 2 in which the values used differ from the experimentally based estimates. The parameter estimates are based on reported measurements for individual reactions, and the modifications made here are necessary to generate the correct cell-level or population-level behaviour within the current model network. The interested reader can consult paper I for the rationale behind the modification of each parameter.

We should point out that the modifications that we have introduced do not change the adaptation properties of the system significantly. For example, for the four-step sequential stimulus protocol we obtain the numerical results in figure 2. We see here that the cell adapts well to the 10^4-fold range in the stimulus level. The total secretion over 20 min is approximately 3.5×10^7 molecules.

Table 2. *Dimensionless parameters and their values*

(From I.)

pathway	dimensionless parameters	relation to dimensional parameters	estimated values	values used
stimulus	α_H	$\frac{k_1}{k_5}H(t)$	120 $\mu M^{-1} \times H(t)$	120 $\mu M^{-1} \times H(t)$
	α_1	$\frac{k_{-1}}{k_5}$	7.2	0.8
	α_2	$\frac{k_2[G_s]_T}{k_5}$	2.67	2.67
	α_3	$\frac{k_3}{k_{-2}+k_3}$	1.0	1.0
	α_4	$\frac{k_4[G_s]_T}{k_5}$	26.7	26.7
inhibitory	β_H	$\frac{h_1}{k_5}H(t)$	35.2 $\mu M^{-1} \times H(t)$	35.2 $\mu M^{-1} \times H(t)$
	β_1	$\frac{h_{-1}}{k_5}$	16.0	16.0
	β_2	$\frac{h_2[G_i]_T}{k_5}$	0.16	0.48
	β_3	$\frac{h_3}{h_{-2}+h_3}$	1.0	1.0
	β_4	$\frac{h_4[G_i]_T}{k_5}$	2.0×10^4	2.0×10^4
	β_5	$\frac{h_5}{k_5}$	0.12	0.40
	β_6	$\frac{h_6}{k_5}$	272.0	204.0
cAMP generation	γ_1	$\frac{l_1}{k_5}$	323.2	323.2
	γ_2	$\frac{l_2[UC]_T}{(l_{-1}+l_2)[iPDE]_T}$	0.048	0.048
	γ_3	$\frac{l_{-3}+l_4}{l_3[iPDE]_T}$	57.7	57.7
	γ_4	$\frac{l_4}{k_5}$	800.0	350.0
independent concentrations	c_1	$\frac{[R_s]_T}{[G_s]_T}$	1.0	1.0
	c_2	$\frac{[R_i]_T}{[G_i]_T}$	1.0	1.0
	c_3	$\frac{[R_s]_T}{[G_i]_T}$	0.668	0.668
dependent concentrations	c_4	$\frac{[UC]_T}{[G_s]_T}$	1.0	1.0
	$\frac{c_1}{c_3}$	$\frac{[G_i]_T}{[G_s]_T}$	1.5	1.5

(*b*) *The mathematical model for suspension experiments*

To describe the dynamics of suspensions, we only have to append reactions for the extracellular dynamics and equations for the evolution of extracellular cAMP. The additional reactions arise from the presence of the membrane-bound phosphodiesterase (mPDE) and the phosphodiesterase secreted to the extracellular medium by the Dd cells (ePDE). As iPDE, these phospho-

PHILOSOPHICAL TRANSACTIONS OF THE ROYAL SOCIETY B BIOLOGICAL SCIENCES

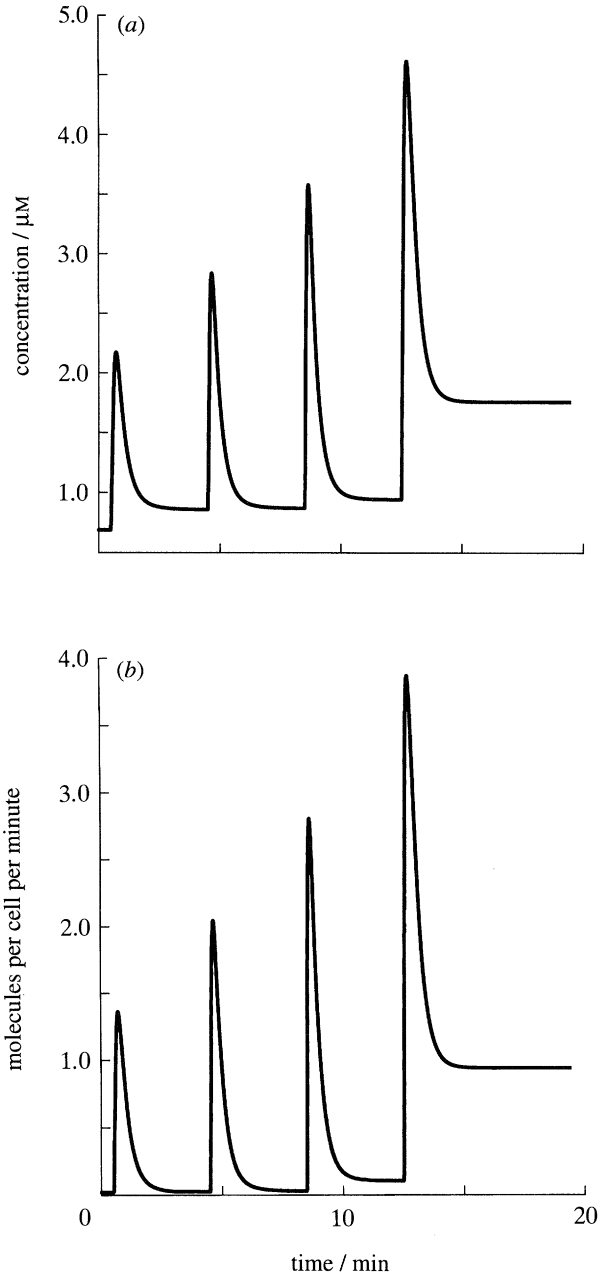

Figure 2. Adaptation to the four-step tenfold increases in stimulus. The system shows good adaptation to the modifications made in the perfusion step. In (*b*), the secretion rate is in 10^6 molecules per cell. The results shown are for $\gamma_2 = 0.175$.

diesterases hydrolyse $cAMP_o$ into adenosine monophosphate (AMP):

$$\left.\begin{aligned} &cAMP_0 + mPDE \underset{l_{-6}}{\overset{l_6}{\rightleftharpoons}} cAMP_0\text{—}mPDE \\ &cAMP_0\text{—}mPDE \xrightarrow{l_7} AMP \\ &cAMP_0 + ePDE \underset{l_{-8}}{\overset{l_8}{\rightleftharpoons}} cAMP_0\text{—}ePDE \\ &cAMP_0\text{—}ePDE \xrightarrow{l_9} AMP. \end{aligned}\right\} \tag{8}$$

Here $cAMP_o$—mPDE denotes the complex between cAMP and phosphodiesterase in the extracellular membrane and $cAMP_o$—ePDE the complex between cAMP and in the extracellular medium. Notice that $cAMP_o$ is different from both H and $cAMP^*_o$ in I.

The additional differential equations are

$$\left.\begin{aligned} V_o\, dy_{14}/dt &= NV_c\, dsr(y_{12}) + NA_c\, l_{-6}\, y_{15} + V_o\, l_{-8}\, y_{16} \\ &\quad - NA_c\, l_6\, y_{14}\, z_8 - NV_c\, l_8\, y_{14}\, z_9, \\ dy_{15}/dt &= -(l_{-6} + l_7)\, y_{15} + l_6\, y_{14}\, z_8, \\ V_o\, dy_{16}/dt &= -V_o(l_{-8} + l_9)\, y_{16} + NV_c\, l_8\, y_{14}\, z_9. \end{aligned}\right\} \tag{9}$$

Here y_{14} stands for $[cAMP_o]$, y_{15} for $[mPDE\text{—}cAMP_o]$, y_{16} for $[ePDE\text{—}cAMP_o]$, z_8 for free [mPDE], z_9 for free [ePDE], V_o for the volume of the extracellular medium, V_c for the volume of a cell, A_c for the surface area of a cell and N for the total number of cells. In addition to the differential equations, there are two other conservation equations, namely,

$$\left.\begin{aligned} &y_{15} + z_8 = [mPDE]_T, \\ &y_{16} + (NV_c/V_o)\, z_9 = (NV_c/V_o)\, [ePDE]_T. \end{aligned}\right\} \tag{10}$$

It is clear that the new introduced variables y_{15}, y_{16} are both positive and bounded. In fact, we have

$$0 \leqslant y_{15} \leqslant [mPDE]_T,\ 0 \leqslant y_{16} \leqslant (NV_c/V_o)\, [ePDE]_T.$$

It follows from this that y_{14} is also bounded.

By scaling the new independent variables and introducing additional non-dimensional parameters, we obtain a non-dimensionalized system for the u_i and v_i. Most of the equations are the same as in I. The newly introduced dimensionless parameters and singular variables are listed in table 3. We use the same scaling for y_{14} as y^*_{14}, namely, $u_7 = y_{14}/(iPDE]_T$.

The newly introduced singular differential equations are

$$\left.\begin{aligned} &\epsilon_7\, dv_7/d\tau = u_8 - v_7 - (1/\gamma_6)\, u_8\, v_7, \\ &\epsilon_8\, dv_8/d\tau = u_8 - v_8 - (1/\gamma_8)\, u_8\, v_8. \end{aligned}\right\} \tag{11}$$

Table 3. *Additional dimensionless variables and parameters*

parameters		variables
$\alpha_0 = \dfrac{k_1[iPDE]_T}{k_5}$	$\gamma_8 = \dfrac{l_{-8} + l_9}{l_8[iPDE]_T}$	$v_7 = \dfrac{(l_{-6} + l_7)\, y_{15}}{l_6[iPDE]_T\,[mPDE]_T}$
$\beta_0 = \dfrac{h_1[iPDE]_T}{k_5}$	$\gamma_9 = \dfrac{l_9[ePDE]_T}{k_5[iPDE]_T}$	$v_8 = \dfrac{(l_{-8} + l_9)\, y_{16}}{l_8[iPDE]_T\,[ePDE]_T}$
$\gamma_6 = \dfrac{l_{-6} + l_7}{l_6[iPDE]_T}$	$\epsilon_7 = \dfrac{k_5}{l_{-6} + l_7}$	
$\gamma_7 = \dfrac{l_7[mPDE]_T A_c}{k_5[iPDE]_T V_c}$	$\epsilon_8 = \dfrac{k_5}{l_{-8} + l_9}$	

PHILOSOPHICAL TRANSACTIONS OF THE ROYAL SOCIETY B BIOLOGICAL SCIENCES

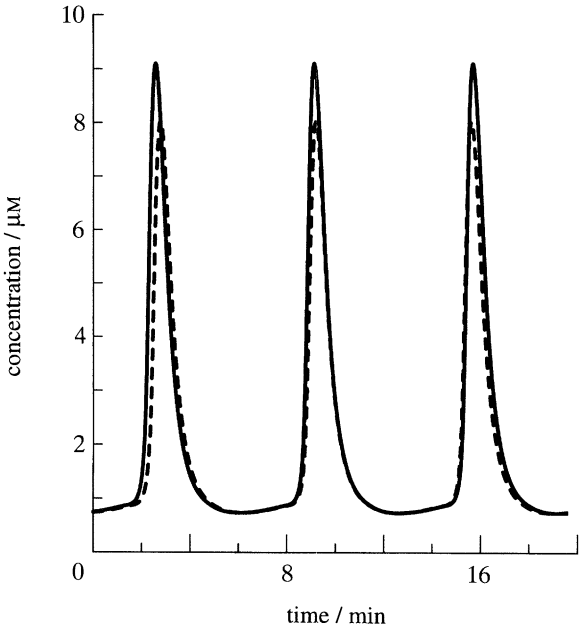

Figure 3. The intracellular concentration for the eight-dimensional system (solid line) and the five-dimensional system (dashed line); $\gamma_2 = 0.25$. Other parameters are as in table 2.

As before we set the time derivatives for the singular variables equal to zero, solve the resulting system, and use the results in the equations for the non-singular variables. The result is that the new non-singular variables satisfy the following system:

$$\left.\begin{aligned} \mathrm{d}u_1/\mathrm{d}\tau &= \alpha_0 u_8 - (\alpha_0 u_8 + \alpha_1) u_1 \\ &\quad + (\beta_5 - \alpha_0 u_8) u_6 - \beta_4 u_1 u_5, \\ \mathrm{d}u_4/\mathrm{d}\tau &= \beta_0 u_8 - (\beta_0 u_8 + \beta_1) u_4, \\ \frac{\mathrm{d}u_8}{\mathrm{d}\tau} &= \frac{\rho}{1-\rho}\left(sr(u_7) - \gamma_7 \frac{u_8}{u_8+\gamma_6} - \gamma_9 \frac{u_8}{u_8+\gamma_8}\right). \end{aligned}\right\} \quad (12)$$

Here ρ is the ratio of cell volume to the total volume in an experiment, i.e.

$$\rho = NV_c/(NV_c + V_o).$$

(*c*) *Reduction from eight variables to five*

The model for suspensions (and for distributed systems as well) involves eight variables. This makes the computation of travelling waves very time-consuming, and we seek further reductions in the number of variables that do not significantly alter the dynamics of the model. The numerical values of the parameters in table 2 and the scaling of the variables suggest that the equations for u_1, u_2 and u_4 can be removed by singular perturbation, even though they do not vary as rapidly as those removed in the first reduction done in I. If one does this the resulting system is five-dimensional, which reduces the computational effort significantly. To check the validity of this reduction we compare the periodic solutions computed for the same parameter values in the eight- and five-dimensional systems in figure 3. One sees that the amplitude is somewhat lower and the period is somewhat shorter in the reduced system. However this reduction does not introduce any significant change in the dynamics.

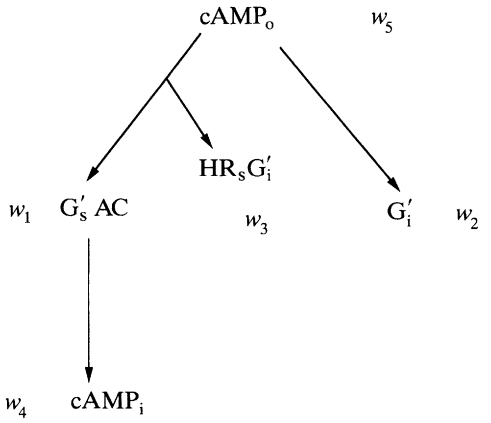

Figure 4. The network for the five-dimensional reduced system. The symbols w_j denote the dimensionless concentrations of the corresponding dimensional quantities.

Further inspection of the equations suggests that the equation for u_6 can also be removed, since the parameter β_4 is large. However, this cannot be done, because the associated term in the u_6 equation varies over three orders of magnitude and thus cannot be uniformly scaled. As a result, we find that the variation of $\dot{u}_6$ along the solution shown in figure 3 is significant over much of the orbit. Thus we are left with a reduction from eight variables to five. This reduces the network shown in figure 1 to that shown in figure 4. To eliminate confusion, we introduce the symbols w_i to denote the remaining variables, and then have the final form of the reduced system,

$$\left.\begin{aligned} \mathrm{d}w_1/\mathrm{d}\tau &= \alpha_4 u_2 (1 - w_1) - w_1, \\ \mathrm{d}w_2/\mathrm{d}\tau &= \beta_2 \beta_3 c_2 u_4 (1 - w_2 - c_3 w_3) \\ &\quad - \beta_5 w_2 + \beta_6 c_3 w_3 - c_3 \beta_4 u_1 w_2, \\ \mathrm{d}w_3/\mathrm{d}\tau &= -(\beta_5 + \beta_6) w_3 + \beta_4 u_1 w_2, \\ \mathrm{d}w_4/\mathrm{d}\tau &= \gamma_1 \gamma_2 w_1 + \gamma_5 (1 - w_1) - \gamma_4 \frac{w_4}{w_4 + \gamma_3} - sr(w_4), \\ \mathrm{d}w_5/\mathrm{d}\tau &= \frac{\rho}{1-\rho}\left(sr(w_4) - \gamma_7 \frac{w_5}{w_5+\gamma_6} - \gamma_9 \frac{w_5}{w_5+\gamma_8}\right). \end{aligned}\right\} \quad (13)$$

Here

$$u_1 = \frac{\alpha_0 w_5 + (\beta_5 - \alpha_0 w_5) w_3}{\alpha_1 + \alpha_0 w_5 + \beta_4 w_2},$$

$$u_2 = \frac{\alpha_2 \alpha_3 c_1 u_1 (1 - w_1)}{1 + \alpha_4 + \alpha_2 \alpha_3 c_1 u_1 - \alpha_4 w_1},$$

$$u_4 = \frac{\beta_0 w_5}{\beta_1 + \beta_0 w_5}.$$

(*d*) *Parameter values*

The switching concentration used in $dsw = 0.87\,\mu\mathrm{M}$. This is in the range of basal cAMP concentration from experiments. If the cAMP concentration is lower than

Table 4. *Estimated values of the new dimensionless parameters*

$\gamma_5 = 0.3$	$sr_1 = 0.02$	$sr_2 = 0.65$	$sw = 0.5$
$\alpha_0 = 312.0$	$\gamma_6 = 11.6$	$\gamma_8 = 750.0$	$\rho = 0.14$
$\beta_0 = 61.0$	$\gamma_7 = 36.7$	$\gamma_9 = 659.3$	

dsw, the cell will not secrete cAMP vigorously. We use $dsr_1 = 6.25 \times 10^{-4}$ s^{-1}, and the active secretion rate as 0.028 s^{-1}. We assume that without an extracellular stimulus the steady state level of $cAMP_i$ is *ca.* 0.6 μM, which is close to what is experimentally measured and is just below the switching concentration for the secretion rate.

The new parameters to be estimated for the suspension experiments are $V_{\max}^{\mathrm{mPDE}}$, K_{mPDE}, $V_{\max}^{\mathrm{ePDE}}$, and K_{ePDE}, where

$$\left.\begin{aligned} V_{\max}^{\mathrm{mPDE}} &= l_7[\mathrm{mPDE}]_{\mathrm{T}}, \\ K_{\mathrm{mPDE}} &= (l_{-6}+l_7)/l_6, \\ V_{\max}^{\mathrm{ePDE}} &= l_9[\mathrm{ePDE}]_{\mathrm{T}}, \\ K_{\mathrm{ePDE}} &= (l_{-8}+l_9/l_8. \end{aligned}\right\} \qquad (14)$$

The value of K_{mPDE} has been reported in Green & Newell (1975) to be around 20.0 μM, which will be used in this paper. The values of other parameters have been estimated in Rapp *et al.* (1985) and Monk & Othmer (1989) and will be used here. They are $V_{\max}^{\mathrm{mPDE}} = 1.67 \times 10^6$ molecules cell^{-1} s^{-1} $= 7.29 \times 10^{-3}$ μmol^{-1} m^{-2} and $V_{\max}^{\mathrm{ePDE}} = 3 \times 10^7$ molecules cell^{-1} s^{-1} $= 7.15 \times 10^4$ μmol^{-1} m^{-3} and K_{ePDE} = 1.3 mM. A typical value for the density in suspensions was estimated as $\rho = 0.14$ in Monk & Othmer (1989), but it may vary, and its influence on the dynamics will be studied later. The dimensionless parameter values from the above estimated parameters are given in table 4.

3. THE DYNAMICS OF SUSPENSIONS

There are several parameters that vary, depending either on the developmental stage of the cells or the experimental setup. The primary parameters studied here are the total amount of adenylate cyclase in a cell, the decay rate of the complex G_i', and the density ρ of cells in a suspension. In dimensionless form, the amount of adenylate cyclase is reflected in γ_2. After starvation, γ_2 increases as a cell develops, and three types of qualitatively distinct dynamics have been found in numerical simulations of suspensions for different values of γ_2. When γ_2 is small the system is not excitable, as judged by the amplification of a cAMP pulse. As γ_2 increases the cells become excitable and hence relay-competent. Finally a stable oscillation arises when γ_2 exceeds a critical value, and the stable oscillatory response persists over a wide range of γ_2. This behaviour matches the experimentally observed stages of Dd cells. The decay rate of G_i' is reflected in the parameter β_5 and, as we shall see later, this is the primary determinant of the frequency of the oscillations, for it determines the recovery rate following removal of an extracellular stimulus. The cell density is reflected in the dimensionless parameter ρ, which we set at 0.18 unless otherwise stated.

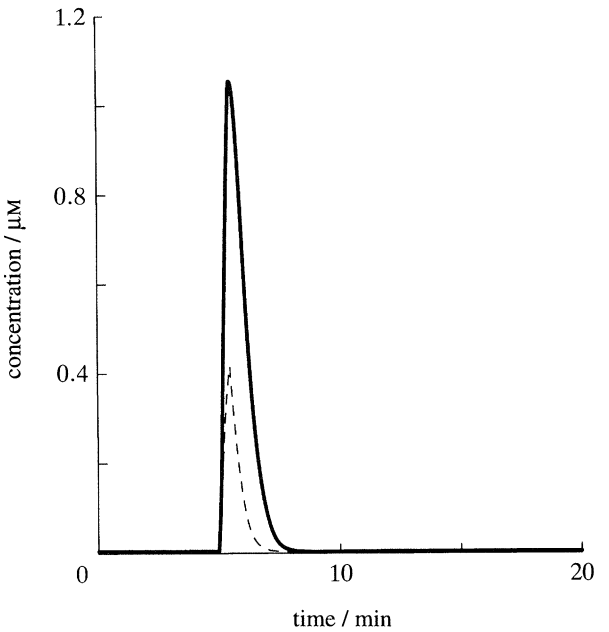

Figure 5. Signal amplification in response to pulse stimuli. Two cell populations in different developmental stages are compared here. For $\gamma_2 = 0.048$ (dashed line) cells are in an early stage and the amplification capacity is small. As the cells express more adenylate cyclase, amplification increases greatly as shown by the solid line, which is for $\gamma_2 = 0.175$. The cAMP stimulus for both is a square wave of amplitude 0.1 μM and duration 0.5 min applied at 5 min.

(*a*) *Signal amplification and refractoriness*

Dd cells that are 4–8 h post-starvation can respond to a small stimulus of extracellular cAMP by generating and secreting cAMP. Secreted cAMP can induce further cAMP release from the same or neighbouring cells, and in this way the initial extracellular signal is amplified by a positive feedback loop. As cells develop after starvation, their ability to amplify signals increases, and in the model this corresponds to an increase in γ_2. A typical signal amplification response is given in figure 5, where an extracellular stimulus of magnitude 0.1 μM is applied at $t = 5$ min for 0.5 min duration. When the cells are in an early stage ($\gamma_2 = 0.048$, as in I), the amplification is small, but it rises with γ_2. When $\gamma_2 = 0.048$ the peak extracellular value is 0.41 μM, while if $\gamma_2 = 0.175$ the peak extracellular value is 1.09 μM. Thus the relative amplification factor is about 2.6.

For a fixed γ_2, the intensity of the response to a stimulus is determined by the strength and duration of that stimulus. In figure 6 we show the responses for fixed $\gamma_2 = 0.175$ and different concentrations in the stimulus. At stimulus levels of 0.001, 0.005, 0.01 and 0.1 μM min^{-1}, the corresponding maximum extracellular cAMP levels reached are 0.09, 0.38, 0.62 and 1.09 μM. From this we see that, although this system is excitable in the usual sense, the threshold for cAMP stimuli is not sharp; as the intensity of the stimulus increases the secretion rate and hence the extracellular cAMP increases in a graded manner. This is similar to what is observed in cardiac myocytes, where the cytoplasmic calcium concentration increases in a graded manner in response to calcium stimuli that

PHILOSOPHICAL TRANSACTIONS OF THE ROYAL SOCIETY B BIOLOGICAL SCIENCES

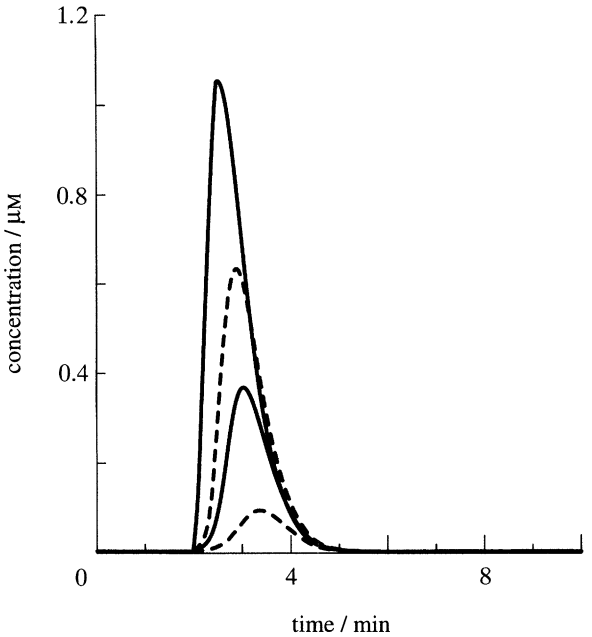

Figure 6. Graded responses of extracellular cAMP as a function of different levels of cAMP stimuli. Square wave stimuli of extracellular cAMP of two different amplitudes are applied at $t = 2$ min for 0.5 min duration. No clear threshold exists for the system. The amplitudes of the stimuli are 0.001 (lower dashed line), 0.005 (lower solid line), 0.01 (upper dashed line) and 0.1 (upper solid line); $\gamma_2 = 0.175$ for all.

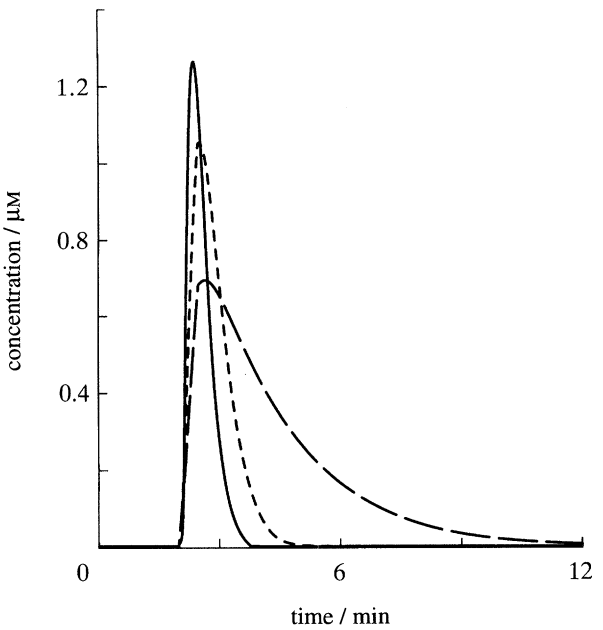

Figure 7. The effect of the cell density on the amplification. A square wave stimulus is applied to a suspension at $t = 2$ min for 0.5 min; $\rho = 0.036$ (broken line), 0.18 (dashed line) and 0.9 (solid line). As cell density increases, there is a significant increase in the extracellular cAMP.

cause release of calcium from the sarcoplasmic reticulum (Stern *et al.* 1992; Tang & Othmer 1994*b*).

Since the amount of mPDE and ePDE varies with the density of cells in the suspension, the response profile should as well. This is shown in figure 7, from which one can infer that the amplitude–duration relation for a fixed stimulus depends strongly on the

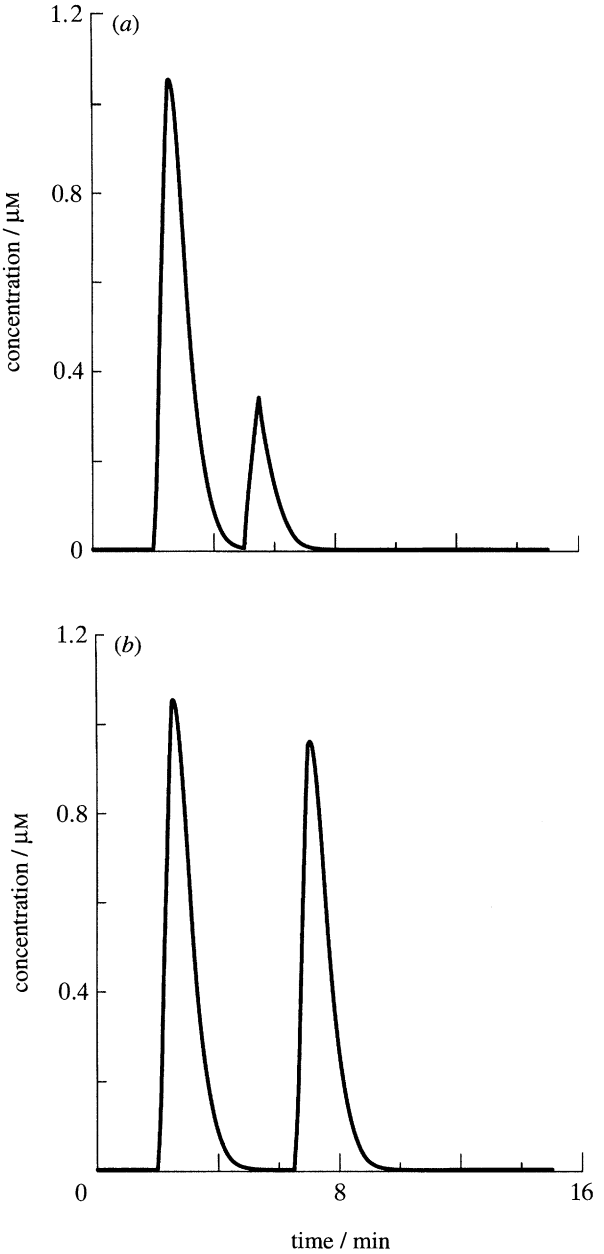

Figure 8. A probe of the refractory period for paired stimuli of equal amplitude. In (*a*) the interstimulus interval is 3 min and in (*b*) it is 4.5 min. In both panels the amplitude of the pulse is 0.1 μM.

cell density. When the cell density is 0.036, the peak extracellular cAMP reached in response to a stimulus of amplitude 0.1 μM is 0.68 μM, which increases to *ca.* 1.09 μM at $\rho = 0.18$ and 1.28 μM at $\rho = 0.8$. The duration of a response decreases as the cell density increases, as could be predicted, since a higher cell density produces a higher concentration of mPDE per unit extracellular volume, and this leads to more rapid hydrolysis of extracellular cAMP. As we shall see later, this has a significant effect on the frequency of oscillations in suspensions. However, the duration of the intracellular cAMP profiles for different density suspensions is similar, since the cell adapts to the extracellular cAMP quickly.

Once stimulated, excitable systems must recover before they can produce a significant response to another stimulus, and the length of this refractory

PHILOSOPHICAL TRANSACTIONS OF THE ROYAL SOCIETY B BIOLOGICAL SCIENCES

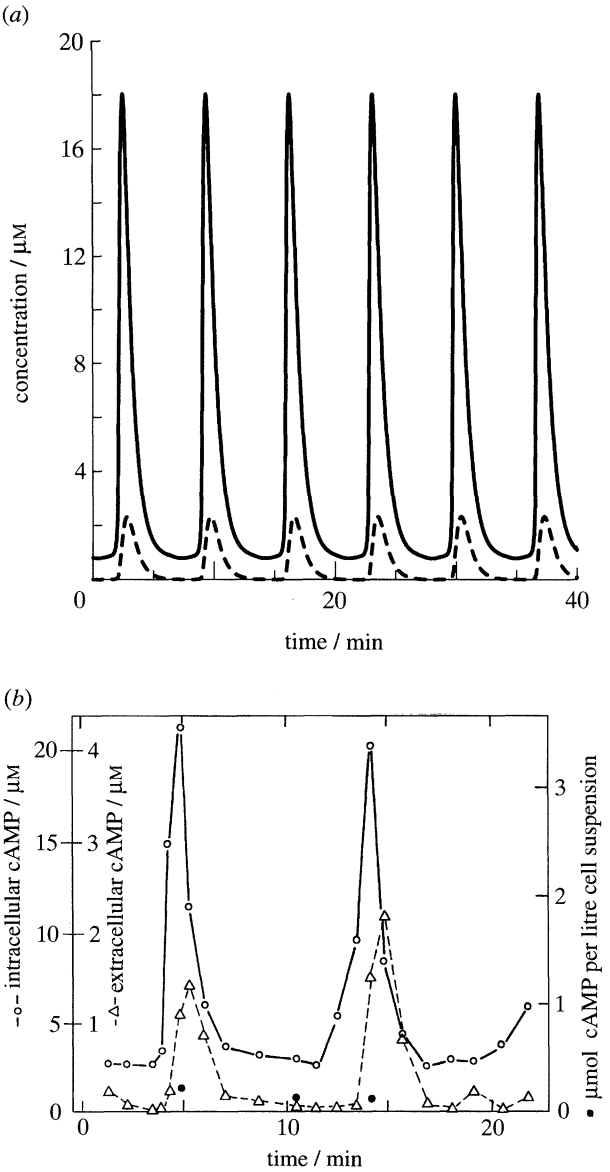

Figure 9. (*a*) Periodic oscillations in a numerical simulation of suspension experiments for $\gamma_2 = 0.4$. Solid lines, intracellular cAMP; dashed line, extracellular cAMP. (*b*) Experimental measurements of intracellular (○) and extracellular (△) cAMP concentration. Redrawn from figure 2 of Gerish & Wick (1975).

period depends on the amplitude of the second stimulus. In figure 8, we show that the refractory period for paired stimuli of the same magnitude is between 3 and 4.5 min. A stimulus applied at 3 min after the first stimulus only produces a small response, but a stimulus of the same amplitude applied 4.5 min after the first stimulus elicits a full scale response. However, the refractory period depends on the strength of a stimulus as well and, if we increase the stimulus magnitude at 3 min after the first stimulus to 1.0 μM min^{-1}, then a full scale response is produced (results not shown). Finally, as we remarked earlier, the length of the recovery period is primarily determined by the value of β_5. A stimulus protocol similar to that used in figure 7, but for $\beta_5 = 0.2$, leads to a refractory period greater than 5 min (results not shown).

(*b*) *Periodic oscillations*

As cells age the amount of adenylate cyclase expressed increases, and for sufficiently large γ_2 a suspension oscillates periodically, as is shown in figure 9*a*. In this figure the time delay between a peak of the intracellular cAMP and the extracellular cAMP is about 0.5 min, which agrees with the experimental results reported in Gerisch & Wick (1975) and Roos *et al.* (1977). The amplitudes of the oscillations are in the same range as the experimental data, which are shown in figure 9*b*.

The periodic solutions have been computed for the entire range of γ_2, for fixed values of the remaining parameters, by using the numerical bifurcation software AUTO (Doedel & Kernevez 1986). The results are shown in figure 10, where in (*a*) we show the amplitude of steady states and periodic solutions and in (*b*) we show the period of the periodic solutions. The periodic solutions emerge via a supercritical Hopf bifurcation at $\gamma_2 \approx 0.177$ and disappear via a supercritical Hopf bifurcation at $\gamma_2 \approx 0.38$. Note that there is an interval in which the steady state coexists with a stable periodic

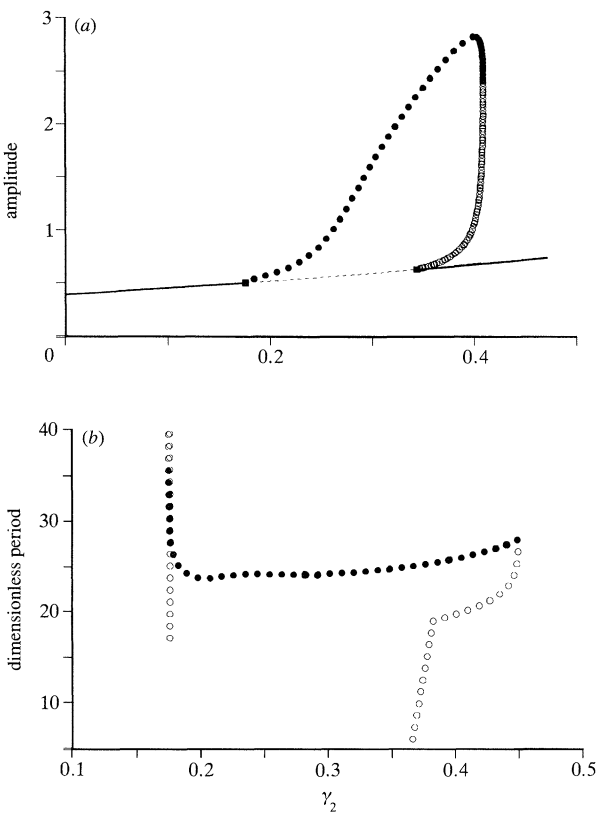

Figure 10. A bifurcation diagram showing the steady states and periodic solutions in a suspension, with γ_2 as the bifurcation parameter. A supercritical Hopf bifurcation occurs at $\gamma_2 \approx 0.177$ and stable periodic solutions arise there. (*a*) Solid/dashed lines denote the amplitude of stable/unstable steady states; solid/open circles denote the amplitude of stable/unstable periodic solutions. For steady states the amplitude is the euclidean norm of the solution; for periodic solutions it is the L_2 norm. To convert the dimensionless concentration to micromolar multiply the numbers on the ordinate by 1.73. (*b*) The dimensionless period of the periodic solutions given in (*a*); to convert the period to minutes divide by 3.75.

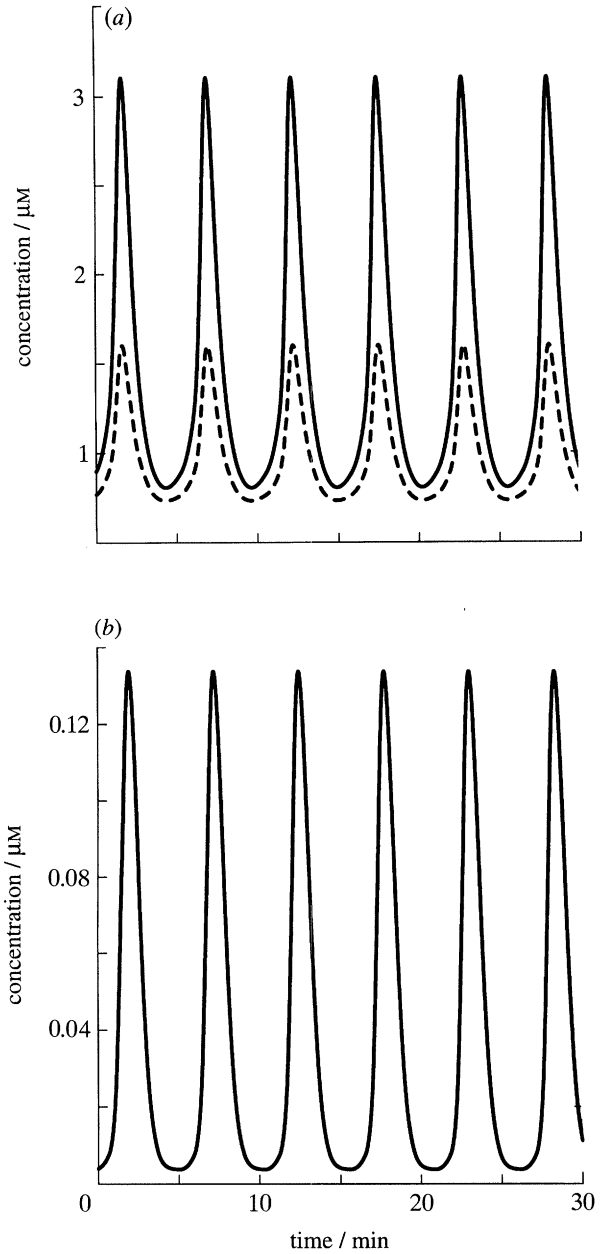

Figure 11. The intracellular (*a*) and extracellular (*b*) cAMP concentrations for a mixed population in suspension. The intracellular concentration is different in the excitable cells (dashed line) and the oscillatory cells (solid line). The population is a mixture of 15% oscillatory cells ($\gamma_2 = 0.45$) and 85% excitable cells ($\gamma_2 = 0.175$).

oscillation. This is consistent with the experimentally observed fact that relay-competent cells at a certain developmental stage may need several pulses of cAMP before they start to oscillate (Gerisch & Hess 1974).

Over a wide range of γ_2 the period lies between 6 and 7 min, which agrees well with most reported values for the wide type Dd cells, but is shorter than the period for experimental results shown in figure 9*b* (Devreotes 1982; Wessels *et al.* 1992).

The results presented thus far are based on the assumption that all cells are in the same developmental stage at any given time, and hence are characterized by the same parameters. However it is also possible that some small fraction of cells become pacemakers and entrain the remainder in suspension experiments.

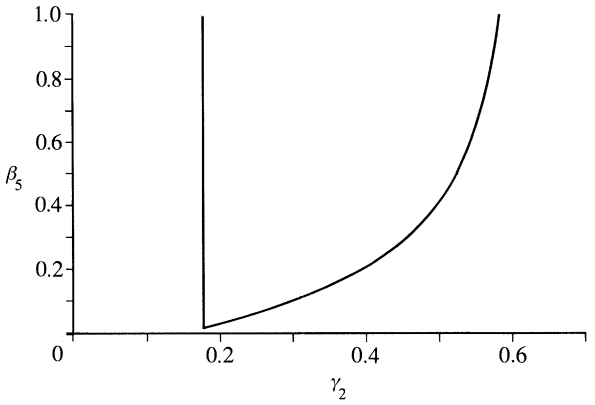

Figure 12. A two-parameter diagram showing the loci of Hopf bifurcation points as a function of γ_2 and β_5. The steady state is unstable in the interior of the wedge-shaped region.

To test this idea numerically, we use two sets of the first four equations in equation (13) to model the intracellular cAMP dynamics for the subpopulations of oscillatory and excitable cells. A single equation for extracellular cAMP is then introduced, with the right side comprising the weighted sum of two terms similar to the right side of equation (13), one for each subpopulation. The entrainment of the excitable cells by the oscillatory cells into a synchronous oscillation using this model is shown in figure 11. In this figure we assume that 15% of the cells have $\gamma_2 = 0.45$, that the remainder have $\gamma_2 = 0.175$, and that all cells have other parameters as before. One sees in the figure that if 15% are pacemakers they can entrain the remainder of the population into a medium amplitude oscillation. The amplitude of extracellular cAMP is reduced from that observed in figure 9, but of course one could reduce the activity of mPDE to compensate for the lower average excitability. This would be reasonable because early stage cells that express less adenylate cyclase also express less mPDE.

(*c*) *The influence of other parameters on the oscillations*

As we indicated earlier, the recovery rate following stimulation is controlled in part by the parameter β_5. This parameter governs the off rate for the inhibitory pathway (see figure 17 of I and discussion there) and, since the off rate of activated G_i is the slowest dynamics in the system, it is easy to understand that the period of oscillation should be sensitive to changes in β_5. This is confirmed by bifurcation computations and simulations (results not shown). At $\beta_5 = 0.2$, the onset of oscillations occurs at a larger value of γ_2, and the amplitude is somewhat smaller. However, the period is substantially longer, which reflects the fact that decreasing β_5 increases the refractory period.

In figure 12 we show a two-parameter diagram of the Hopf bifurcation points as a function of γ_2 and β_5. This figure shows that the onset of oscillations, as measured by the first Hopf bifurcation point for increasing γ_2, is essentially independent of β_5, whereas the second Hopf point depends very strongly on β_5. For sufficiently small β_5 there are no periodic solutions, whereas when they exist, the range of γ_2 over which

PHILOSOPHICAL TRANSACTIONS OF THE ROYAL SOCIETY B BIOLOGICAL SCIENCES

they exist increases with β_5. Thus the faster recovery or shortening of the refractory period produces oscillations at higher rates of cAMP production.

Another important parameter is cell density. Experiments show that suspensions can oscillate at a very low density of cells (Alcantara & Monk 1974). This can be understood if the cells are very sensitive to a cAMP signal, but in any case there is a lower bound to the density at which a suspension can oscillate since extracellular cAMP must reach the threshold level. One finds numerically that the onset of oscillations as a function of γ_2 is essentially independent of the density, except at very low density (results not shown). This conclusion is for homogeneous population of cells, and may change if we assume that only a small fraction of cells are pacemakers. However, an increase in cell density increases both the oscillation frequency and the amplitude (results not shown).

4. WAVE PROPAGATION

The last aspect of Dd dynamics treated here concerns the propagation of waves in a spatially distributed field of cells. We consider both a one-dimensional and a two-dimensional spatial domain, and to obtain a simple mathematical model we make the following assumptions.

There are sufficient cells present in the medium so that the field can be considered as a continuum.
The concentrations of ePDE and mPDE are uniform in space.
Extracellular cAMP is the only diffusible chemical in the system.
The cell density ρ is constant and uniform throughout the domain; the cells are supposed to be immobile.

Thus the analysis applies to the very early stages of aggregation. Results from a model that incorporates cell motion and exhibits the patterns of aggregation seen experimentally will be reported elsewhere (Dallon & Othmer 1995*b*).

Under these assumptions, the governing equations for the extracellular cAMP is

$$\frac{\partial w_5(x,t)}{\partial \tau} = D\Delta w_5 + \frac{\rho}{1-\rho}\left(sr(w_4) - \frac{\gamma_7 w_5}{w_5+\gamma_6} - \frac{\gamma_9 w_5}{w_5+\gamma_8}\right), \tag{15}$$

where D is the dimensionless diffusion rate constant for cAMP and Δ is the laplacian operator. The dimensional diffusion coefficient D_0 is estimated at 5.0×10^{-6} cm^2 s^{-1} by Cohen & Robertson (1971*a*, *b*), but we shall use $D = 2.5\times10^{-6}$ cm^2 s^{-1} throughout our calculations. The dimensionless diffusion coefficient is defined as $D \equiv D_0/k_5L^2$ where L is a characteristic dimension of the system. The remaining equations are the same ordinary differential equations as are given in (13), except that all the variables are functions of both time t and space x. We shall use a homogeneous Neumann (no-flux) boundary condition in all simulations, which corresponds to cells spread on an agar surface embedded in a Petri dish.

The density of cells is typically around 10^5 cells cm^{-2} in wave propagation experiments. The lower limit of the density for propagation is *ca.* 2.5×10^4 cells cm^{-2}, and the largest density used in *ca.* 10^6 cells cm^{-2} (Alcantara & Monk 1974; Tomchik & Devreotes 1981). If we use the conversion procedure given in Monk & Othmer (1990), this gives a range for the dimensionless density ρ of 0.031 to 1.25. A value for ρ higher than 1 simply means that more than one layer of cells is present on average, and depends of course on the assumptions made in the conversion. The standard value we use in the following simulations is $\rho = 0.14$, or 1.12×10^5 cells cm^{-2}, except where otherwise noted.

Table 5. *The wave speed as a function of* γ_2

γ_2	speed (μm min^{-1})
0.155	0
0.16	218
0.17	306
0.175	338

(*a*) *Travelling waves in one-dimensional space*

First consider a one-dimensional system of length 1 cm, which we denote [0, 1] in dimensionless form. As we showed in the context of suspensions, the parameters γ_2 and ρ have a significant effect on the dynamics, and the same can be expected in aggregation fields. In the results reported below we choose the parameters as in table 2 except for γ_2, which is specified as follows. In the interval [0, 0.05] we set $\gamma_2 = 0.4$ to make cells in that interval pacemakers, were they to be placed in a suspension at the same density. In the interval [0.15, 1.0] we set γ_2 so as to make the cells excitable, and we then interpolate between these regions with a cubic spline. Thus the pacemaker region initiates waves periodically, and if the medium is sufficiently excitable they propagate throughout the interval.

The effect of changes in the excitability in the driven portion of the field is shown in table 5, where we give the wave speed as a function of the excitability. Alcantara & Monk (1974) report speeds in the range of 200–400 μm min^{-1} for the first wave through a medium and lower speeds for later waves, while Siegert & Weijer (1989) report speeds in the range 300–600 μm min^{-1}. As the cells progress in development the wave speed increases, and this is reflected in the model by the change in γ_2: as γ_2 increases, the system becomes more excitable and can support more rapidly propagating waves. The values given in table 5 reflect the steady state wave speed for the given parameters, which is achieved after several waves have passed through the interval. Where propagation fails the medium may propagate a single wave and then block succeeding waves.

The density of cells in the aggregation field also has a significant effect on the speed, as is shown in figure 13. The lower cutoff for propagation is $\rho = 0.05$, which is slightly higher than the observed value of 0.03. In figure 14 we show the intra- and extracellular cAMP at two points in the interval as a function of time. The

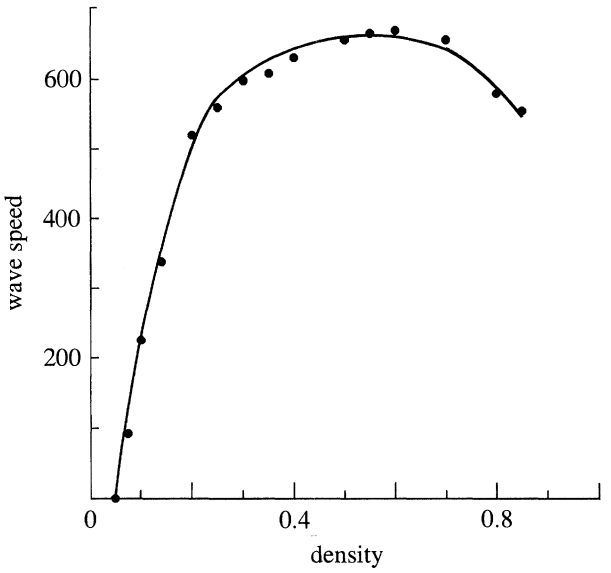

Figure 13. The influence of the density on wave speed. To convert the density to cells per square centimetre multiply the number on the abscissa by 8×10^5. The filled circles represent the computed values. All parameters except the density and γ_2 have the values used in table 2; $\gamma_2 = 0.175$ in the interval [0.15, 1.0].

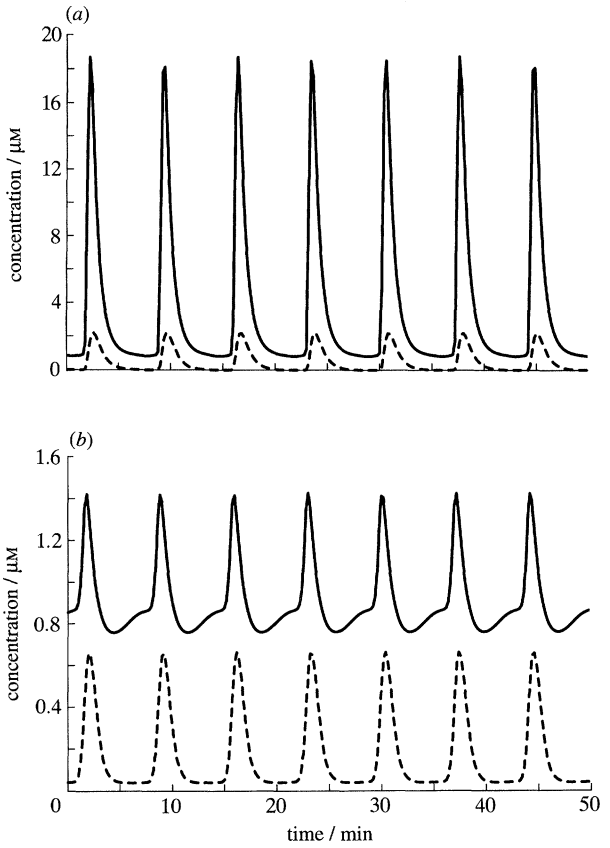

Figure 14. The intra- and extracellular cAMP as a function of time at (*a*) $x = 0.1$ and (*b*) $x = 0.5$ for the travelling wave corresponding to $\rho = 0.15$ in figure 13. Other parameters are as in table 2. In (*a*) solid lines denote the intracellular cAMP concentration and dashed lines denote the extracellular cAMP concentration. In (*b*) the dashed line denotes ten times the extracellular cAMP concentration.

pacemaker region (figure 14*a*) generates a large amplitude wave, but the excitable region (figure 14*b*) propagates a wave of much smaller amplitude. The peak average cAMP concentration in the field is 0.24 μM in figure 14*b*, which is in the range reported by Tomchik & Devreotes (1981). At higher cell densities the amplitude of extracellular cAMP increases significantly, just as in suspensions.

(*b*) *Two-dimensional patterns*

Various mathematical models of the single cell dynamics have been used for the purpose of simulating the observed two-dimensional wave patterns (Othmer & Monk 1988; Tyson & Murray 1989; Foerster *et al.* 1990; Othmer 1990). In particular, Monk & Othmer (1990) showed that, if a model represents the stimulus–response behaviour of an individual cell correctly, then the wave patterns will also be reproduced. In this section, some of the simulations of two-dimensional wave patterns from the present model are shown. As we shall see, the results also agree well with the experimental results shown in figure 15, which demonstrates once again that these aspects will follow if the input–output behaviour of the cell is correct.

In figure 16 we show a stable spiral wave computed on a 1.5 cm × 1.5 cm domain, using the parameters corresponding to the excitable region in figure 14. The computed wave was initiated by using a broken plane wave for initial data in a narrow strip extending halfway across the region, while setting the remainder of the region to the rest state. The period of this spiral is approximately 5.8 min and the wave speed is 460 μm min^{-1} far from the centre, which gives a spatial wave length of about 2.3 mm. The radius of the core is *ca.* 0.1 mm. These results are in the range of experimental results obtained by Gross *et al.* (1976), by Tomchik & Devreotes (1981), and by Siegert & Weijer (1989).

Another commonly observed wave pattern in experiments is a pair of coexisting co- or counter-rotating spiral waves (cf. figure 15*b*). In figure 17, we show two cases of such coexistence obtained from numerical simulations. In figure 17*a* we show two co-rotating spirals, each rotating in a clockwise direction on a domain 2.0 cm × 2.0 cm, and in figure 17*b* we show a pair of counter-rotating spirals. The initial data are similar to those used for generating one spiral wave, except that two stripes from the boundary are used for co-rotating spirals and one stripe in the centre is used to generate counter-rotating spirals. Far from the centre both types of spiral produce an approximately elliptical wavefront.

The large proportion of spiral waves observed in experiments is undoubtedly due to the inhomogeneity of the medium rather than to any special initial conditions. The cell density may not be uniform, the developmental stage of cells in the agar may be different, the cell population may not be homogeneous genetically and the cells are mobile. Computations in which the cells are allowed to aggregate show that it is very easy to generate spirals under these conditions even when cells are identical (Dallon & Othmer 1955*a*).

PHILOSOPHICAL TRANSACTIONS OF THE ROYAL SOCIETY B BIOLOGICAL SCIENCES

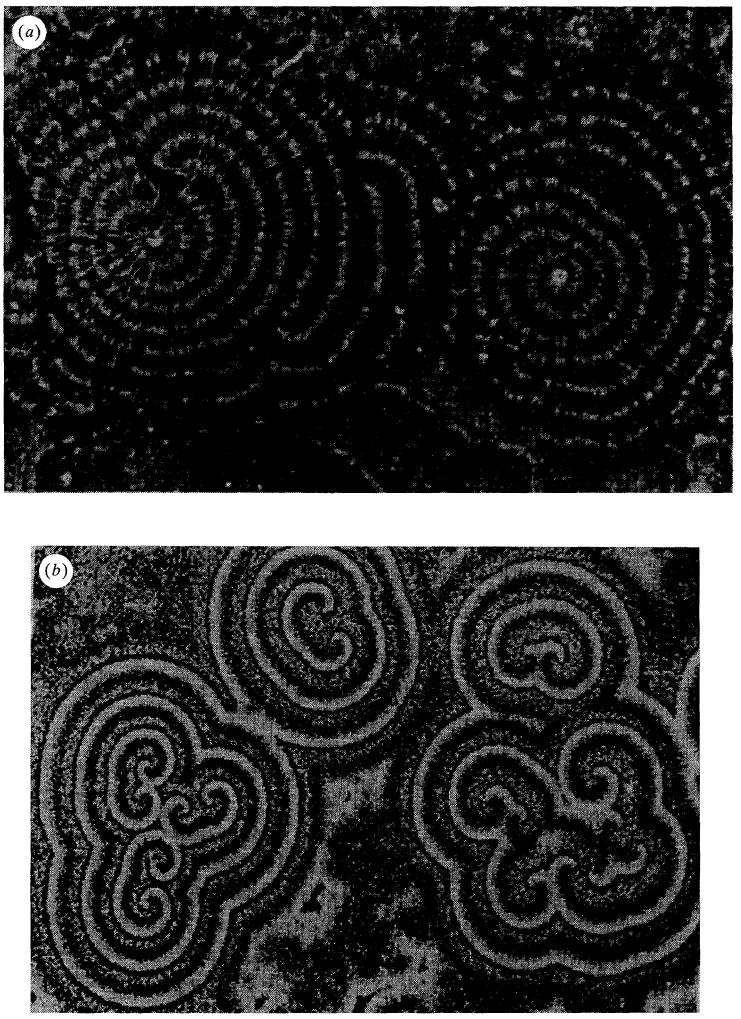

Figure 15. Spiral waves in aggregation fields of *Dictyostelium discoideum*. (*a*) From Newell (1983). (*b*) From Siegert & Weijer (1989).

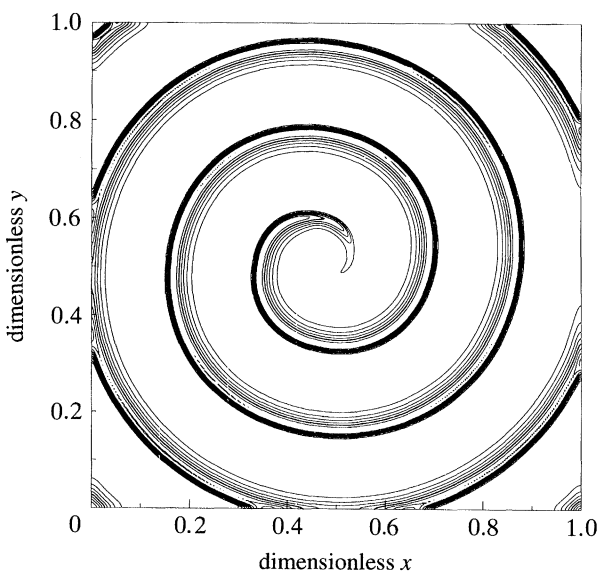

Figure 16. A single spiral wave in a 1.5 cm × 1.5 cm square. Shown here are the contours of extracellular cAMP concentration. The spiral wave is rotating clockwise around the core region. Throughout the square, $\gamma_2 = 0.175$.

Target patterns are also commonly observed in experiments. In figure 18, we show the results of a two-dimensional computation with three oscillating centres in a 2.0 cm × 2.0 cm space. In the scaled space, the fastest pacemaker is centred around (0.25, 0.5), with a period of 6.2 min. The two slower pacemakers are centred at (0.75, 0.25) and (0.75, 0.75), respectively. The radii for all three pacemakers are 0.05. The parameter values for these three centres are $\gamma_2 = 0.25$, 0.35 and 0.45. The period for the lower centre is 6.8 min and the upper pacemaker 7.1 min. Because we cannot show the computation in continuous time, only a snapshot from one fixed time is given here. We can see how the waves initiated by the faster pacemaker dominate the excitable region far from the centre and how the slow pacemaker changes the travelling front of the waves from the faster pacemaker. However the faster pacemaker never completely entrains the slower ones when the cells are immobile, but when cell movement is included the faster one may effectively control of the entire field.

5. CONCLUSION

In this paper we have modified and reduced a model for signal transduction via G proteins first developed in Tang & Othmer (1994*a*). We introduced a basal

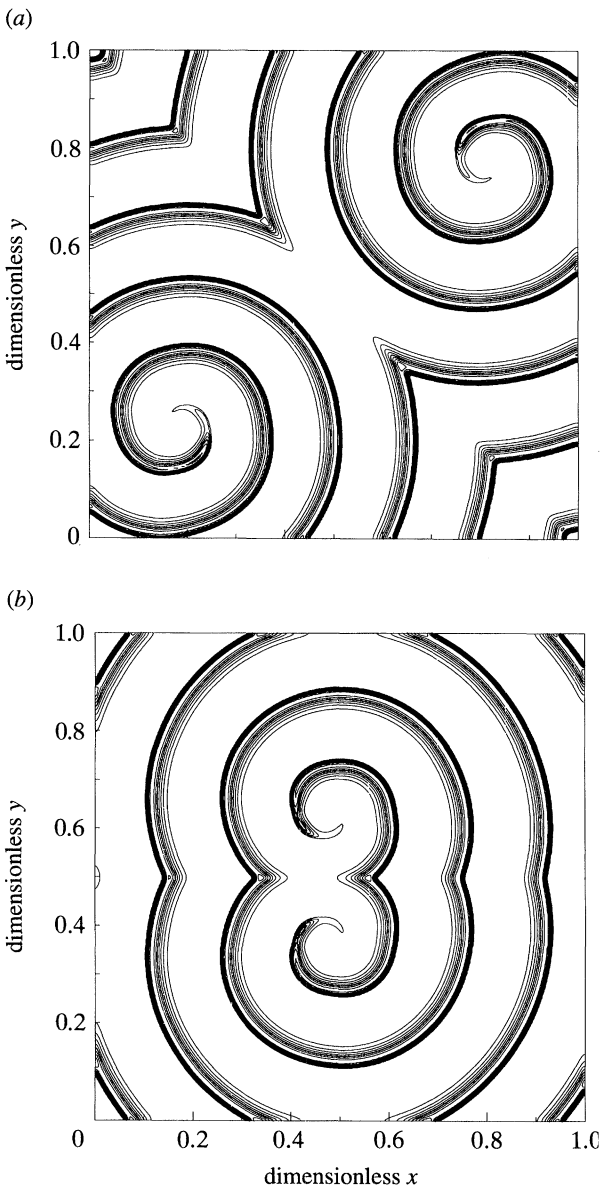

Figure 17. The coexistence of two spirals in a 2.0 cm × 2.0 cm space. In (*a*) ($t = 38$ min) the two spiral waves are co-rotating, while in (*b*) ($t = 30$ min) they are counter-rotating. See figure 15 for the experimental result.

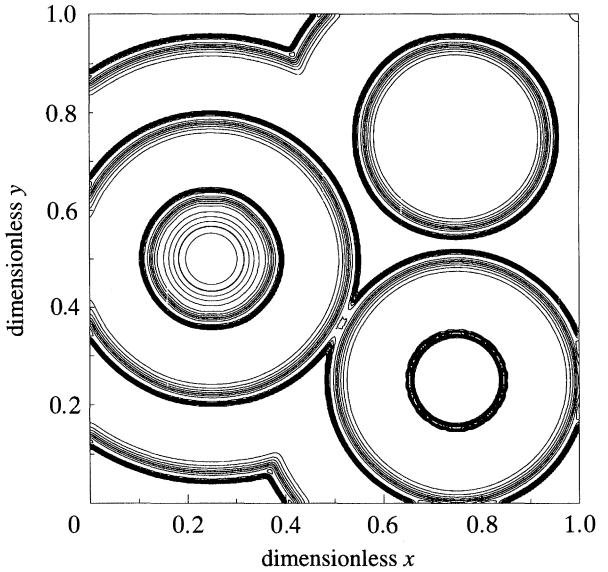

Figure 18. Three interacting pacemakers in a 2.0 cm × 2.0 cm domain. The fastest pacemaker dominates wave propagation far from the centre, but all persist. The slower pacemakers cause a local change in the curvature of travelling wave fronts. Time $t = 47$ min from the onset of oscillation.

secretion rate for cAMP and modified the secretion rate function, and we then reduced the number of essential variables from eight to five. This model can reproduce the observations from a variety of experimental configurations, including perfusion experiments, suspension experiments and wave propagation experiments. It is shown that by changing a single bifurcation parameter, which is believed to change as the cell develops, the model can give rise to signal amplification, excitability and oscillations. In addition, when spatial differences in the cAMP concentrations are admitted, the model can give rise to axisymmetric waves and single or multiple spiral waves. The wave speed, period and amplitude are in good agreement with the experimental results.

Following starvation Dd cells initiate an elaborate developmental program that includes changes in several of the major enzymes (Othmer *et al.* 1995). We assume that one major event in this developmental program is to increase the expression of the gene that codes for adenylate cyclase, which is reflected in the parameter γ_2 in the model (cf. table 2). In reality the cells may increase the receptor concentrations and the G protein concentration as well as the adenylate cyclase concentration, and these changes would be reflected in several other parameters in the model (cf. table 2). We tested by computation the scenario in which the receptor concentration, the G protein level and the adenylate cyclase increase simultaneously with the same proportions and found that the numerical results are very similar to those obtained when only the adenylate cyclase concentration is increased.

As we noted in I, there is uncertainty in our current knowledge of the G proteins in Dd. We postulated that the α-subunit activates the cyclase and that G_i' acts at the level of HR_s. However, direct interaction between G_i' and adenylate cyclase (AC) is also possible and may give the correct system dynamics (Tang & Othmer 1994*a*). Thus a model with this type of interaction may very well give much the same behaviour as does the present model when the extracellular dynamics are included. However, in our current model, an increase in the concentration of G_i is not required to maintain adaptation if the amount of AC increases, since the total concentration of R_s is not changed. If G_i exerts its inhibitory effect through direct coupling with AC, not HR_s, then proportional changes of G_i are required as the AC concentration increases in order to maintain adaptation. The ATP consumption by G_i will also increase proportionally, which is further theoretical support for our model, in addition to the reasons already adduced in Tang & Othmer (1994*a*).

The basis for postulating that the α-subunit activates the cyclase was our assumption that both G_s and G_i are heterotrimeric proteins with the same βγ-subunits. Recent evidence suggests that it may be the βγ-subunit of G_s that activates the cyclase, either directly or

PHILOSOPHICAL TRANSACTIONS OF THE ROYAL SOCIETY B BIOLOGICAL SCIENCES

through an intermediate species CRAC (cytosolic regulator of adenylate cyclase) (Wu & Devreotes 1994). This could be accommodated in our model by simply changing the identity of the activating species, but it does require that the βγ-subunit of G_i be different from that of G_s, for otherwise the signal would not be turned off. For example, if G_i is a ras-like G protein, then the model can be applied with only minor changes (P. Schaap, personal communication).

The biochemistry for the other components of the model is reasonably well settled. There may be some cross-talk between the cAMP pathway and the IP_3—Ca^{2+} pathway, but this is not included in this model (Mason *et al.* 1971; Klein & Brachet 1975). However, if such interactions exist, they are only secondary, just as is the effect of receptor phosphorylation on the adaptation. Further research on the biochemical aspects will be able to provide a more accurate estimate of parameters involved, but will probably not produce major changes in the general pathways.

The fidelity between the results presented herein and experimental observations suggest that our basic model may serve in later stages of Dd development as well, provided proper account is taken of known changes in the major enzymes (Othmer *et al.* 1995). In this vein, preliminary results show that the model can generate the proper frequencies, wave speeds and cAMP amplitudes under conditions that apply in the slug stage of Dd (Schaap & Othmer 1995).

This research was supported in part by NIH grant number GM29123.

REFERENCES

Alcantara, F. & Monk, M. 1974 Signal propagation during aggregation in the slime mold *Dictyostelium discoideum*. *J. gen. Microbiol.* **85**, 321–334.

Clark, R. L. & Steck, T. L. 1979 Morphogenesis in *Dictyostelium*: an orbital hypothesis. *Science, Wash.* **204**, 1163–1168.

Cohen, M. H. & Robertson, A. 1971*a* Wave propagation in the early stages of aggregation of cellular slime molds. *J. theor. Biol.* **31**, 101–118.

Cohen, M. H. & Robertson, A. 1971*b* Chemotaxis and the early stages of aggregation in cellular slime molds. *J. theor. Biol.* **31**, 119–130.

Dallon, J. & Othmer, H. G. 1995*a* Signal detection and cell orientation in a chemotactic field. (In preparation.)

Dallon, J. & Othmer, H. G. 1995*b* Aggregation patterns in the cellular slime mould *Dictyostelium discoideum*. (In preparation.)

Devreotes, P. N. 1982 In *The development of Dictyostelium discoideum*, pp. 117–168. New York: Academic Press. Chap. Chemotaxis.

Devreotes, P. 1989 Cell–cell interactions in *Dictyostelium* development. *Trends Genet.* **5**, 242–245.

Devreotes, P. N., Derstine, P. L. & Steck, T. L. 1979 Cyclic 3′,5′ AMP relay in *Dictyostelium discoideum* I. A technique to monitor responses to controlled stimuli. *J. Cell Biol.* **80**, 291–299.

Devreotes, P. N. & Steck, T. L. 1979 Cyclic 3′,5′, AMP relay in *Dictyostelium discoideum* II. Requirements for the initiation and termination of the response. *J. Cell Biol.* **80**, 300–309.

DeYoung, G., Monk, P. B. & Othmer, H. G. 1988 Pacemakers in aggregation fields of *Dictyostelium discoideum*. Does a single cell suffice? *J. math. Biol.* **26**, 486–517.

Dinauer, M. C., MacKay, S. A. & Devreotes, P. N. 1980*a* Cyclic 3′,5′ AMP relay in *Dictyostelium discoideum* III. The relationship of cAMP synthesis and secretion during the cAMP signaling response. *J. Cell Biol.* **86**, 537–544.

Dinauer, M. C., Steck, T. L. & Devreotes, P. N. 1980*b* Cyclic 3′,5′ AMP relay in *Dictyostelium discoideum* IV. Recovery of the cAMP signaling response after adaptation to cAMP. *J. Cell Biol.* **86**, 545–553.

Dinauer, M. C., Steck, T. L. & Devreotes, P. N. 1980*c* Cyclic 3′,5′ AMP relay in *Dictyostelium discoideum* V. Adaptation of the cAMP signaling response during cAMP stimulation. *J. Cell Biol.* **86**, 554–561.

Doedel, E. J. & Kernevez, J. P. 1986 AUTO: software for continuation and bifurcation problems in ordinary differential equations. Applied Mathematics Report. California Institute of Technology.

Durston, A. J. 1973 *Dictyostelium discoideum* aggregation fields as excitable media. *J. theor. Biol.* **42**, 483–504.

Foerster, P., Müller, C. & Hess, B. 1990 Curvature and spiral geometry in aggregation patterns of *Dictyostelium discoideum*. *Development* **109**, 11–16.

Gerisch, G., Fromm, H., Huesgen, A. & Wick, Y. 1975 Control of cell-contact sites by cyclic AMP pulses in differentiating *Dictyostelium* cells. *Nature, Lond.* **255**, 547–549.

Gerisch, G. & Hess, B. 1974 Cyclic-AMP-controlled oscillations in suspended *Dictyostelium* cells: their relation to morphogenetic cell interactions. *Proc. natn. Acad. Sci. U.S.A.* **71**, 2118–2122.

Gerisch, G., Malchow, D., Roos, W. & Wick, U. 1979 Oscillations of cyclic nucleotide concentrations in relation to the excitability of *Dictyostelium* cells. *J. exp. Biol.* **81**, 33–47.

Gerisch, G. & Wick, U. 1975 Intracellular oscillations and release of cyclic AMP from *Dictyostelium* cells. *Biochem. biophys. Res. Commun.* **65**, 364–370.

Green, A. A. & Newell, P. C. 1975 Evidence for the existence of two types of cAMP binding sites in aggregating cells of *Dictyostelium discoideum*. *Cell* **6**, 129–136.

Gross, J. D., Peacey, M. J. & Trevan, D. J. 1976 Signal emission and signal propagation during early aggregation in *Dictyostelium discoideum*. *J. Cell Sci.* **22**, 645–656.

Klein, C. & Brachet, P. 1975 Effects of progesterone and EDTA on cyclic AMP phosphodiesterase in *Dictyostelium discoideum*. *Nature, Lond.* **254**, 432–434.

Loomis, W. F. 1992 In *Gene regulation: biology of antisense RNA and DNA*, pp. 197–207. New York: Raven Press.

Mason, J. W., Rasmussen, H. & deBella, F. 1971 3′,5′-AMP and Ca in slime mold aggregation. *Expl Cell Res.* **67**, 156–160.

Monk, P. B. & Othmer, H. G. 1989 Cyclic AMP oscillations in suspensions of *Dictyostelium discoideum*. *Phil. Trans. R. Soc. Lond.* B **323**, 185–224.

Monk, P. B. & Othmer, H. G. 1990 Wave propagation in aggregation fields of the cellular slime mould *Dictyostelium discoideum*. *Proc. R. Soc. Lond.* B **240**, 555–589.

Newell, P. C. 1983 Attraction and adhesion in the slime mold *dictyostelium*. In *Fungal differentiation: a contemporary synthesis* (ed. J. E. Smith), pp. 43–71. New York: Marcel Dekker.

Othmer, H. G. & Monk, P. B. 1988 Concentration waves in aggregation fields of a cellular slime mold. In *Biomathematics and related computational problems* (ed. L. Ricciardi), pp. 381–398. Dordrecht: Kluwer Academic Publishers.

Othmer, H. G., Schaap, P. & Tang, Y. 1995 A model for

pattern formation in *Dictyostelium discoideum* differentiation. *Differentiation*. (In the press.)

Rapp, P. E., Monk, P. B. & Othmer, H. G. 1985 Quantitative estimates of kinetic parameters in the calcium cycle nucleotide network in *Dictyostelium discoideum*. Technical Report of the Department of Physiology and Biochemistry. Medical College of Pennsylvania, Philadelphia.

Robertson, A., Cohen, D. J. & Cohen, M. H. 1972 Control of aggregation in *Dictyostelium discoideum* by an external periodic pulse of cyclic adenosine monophosphate. *Science, Wash.* **175**, 333–335.

Roos, W., Scheidegger, C. & Gerisch, G. 1977 Adenylate cyclase activity oscillations as signals for cell aggregation in *Dictyostelium discoideum*. *Nature, Lond.* **266**, 259–260.

Schaap, P. & Othmer, H. G. 1995 cAMP oscillations and waves in the slug stage of *Dictyostelium discoideum*. (In preparation.)

Schaap, P. & Wang, M. 1993 Four signals to shape a slime mold. In *Experimental and theoretical advances in biological pattern formation* (ed. H. Othmer, P. K. Maini & J. D. Murray), pp. 301–318. Plenum Press.

Siegert, F. & Weijer, C. 1989 Digital image processing of optical density wave propagation in *Dictyostelium discoideum* and analysis of the effects of caffeine and ammonia. *J. Cell Sci.* **93**, 325–335.

Stern, P., Edwards, F. A. & Sakmann, B. 1992 Fast and slow components of unitary EPSCs on stellate cells elicited by focal stimulation in slices of rat visual cortex. *J. Physiol., Lond.* **449**, 247–278.

Tang, Y. & Othmer, H. G. 1994*a* A G-protein-based model of adaptation in *Dictyostelium discoideum*. *Math. Biosci.* **120**, 25–76.

Tang, Y. & Othmer, H. G. 1994*b* A model of calcium dynamics in cardiac myocytes based on the kinetics of ryanodine-sensitive calcium channels. *Biophys. J.* **67**, 2223–2235.

Tomchik, K. J. & Devreotes, P. N. 1981 Adenosine 3′,5′-monophosphate waves in *Dictyostelium discoideum*: a demonstration by isotope dilution-fluorography. *Science, Wash.* **212**, 443–446.

Tyson, J. & Murray, J. 1989 Cyclic AMP waves during aggregation of *dictyostelium* amoebae. *Development* **106**, 421–426.

Wessels, D., Murray, J. & Soll, D. R. 1992 Behavior of *Dictyostelium* amoebae is regulated primarily by the temporal dynamic of the natural cAMP wave. *Cell Motil. Cytoskel.* **23**, 145–156.

Wu, L. & Devreotes, P. N. 1994 The G protein β-subunit is involved in multiple signal transduction pathways in *Dictyostelium*. *Abstracts of the International Dictyostelium Conference*.

Received 15 December 1994; accepted 24 February 1995

PHILOSOPHICAL TRANSACTIONS OF THE ROYAL SOCIETY B BIOLOGICAL SCIENCES

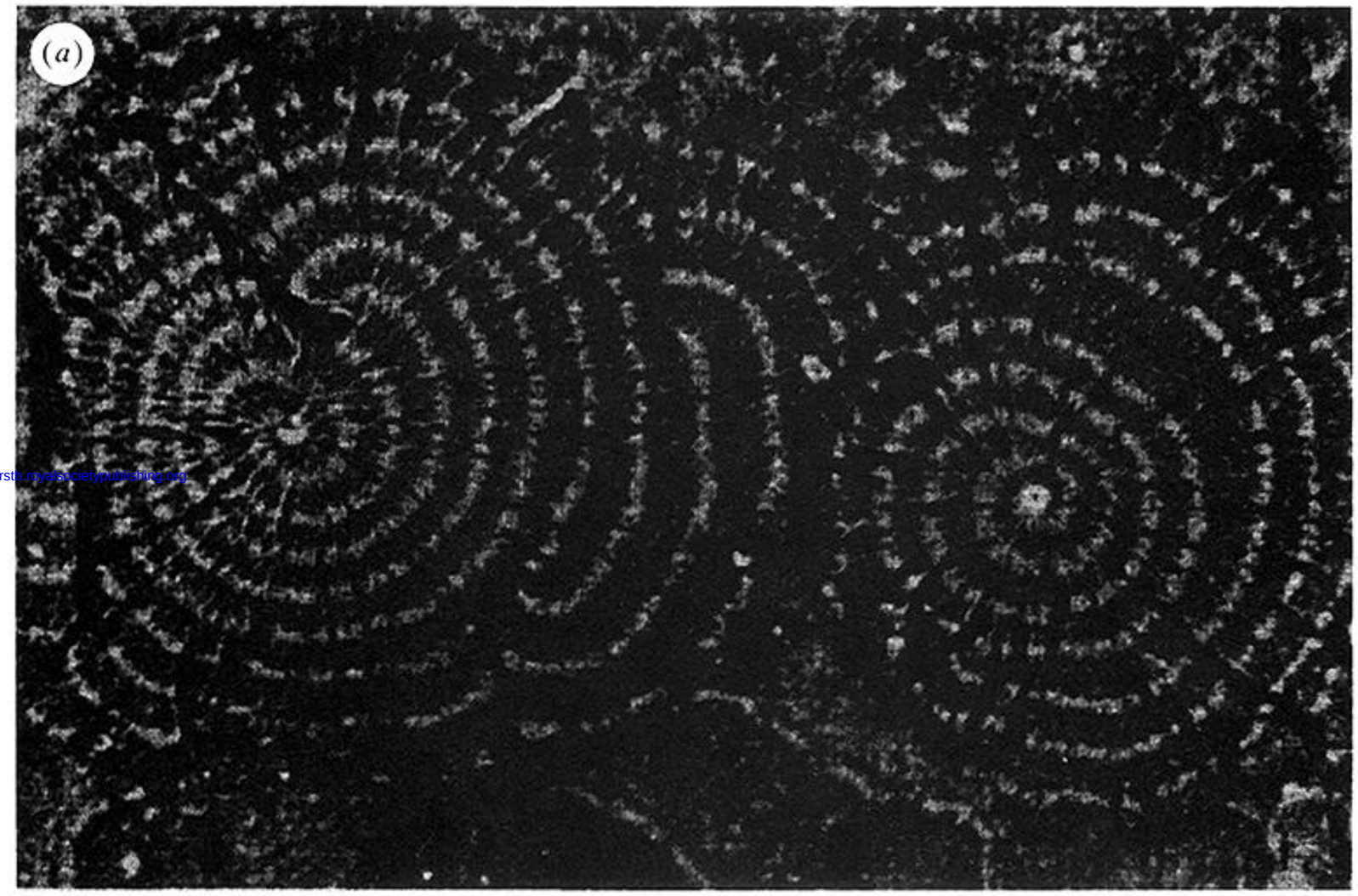

igure 15. Spiral waves in aggregation fields of *Dictyostelium discoideum*. (*a*) From Newell (1983). (*b*) From Siegert & Veijer (1989).